Nanoscale

Adsorption of Alkylamines on Cu Surfaces: Identifying Ideal Capping Molecules Using First-Principles Calculations

Journal:	*Nanoscale*
Manuscript ID	NR-ART-09-2021-005759.R1
Article Type:	Paper
Date Submitted by the Author:	02-Oct-2021
Complete List of Authors:	Chen, Zihao; The Pennsylvania State University University Park, Chemical Engineering Fichthorn, Kristen; Pennsylvania State University,

Adsorption of Alkylamines on Cu Surfaces: Identifying Ideal Capping Molecules Using First-Principles Calculations

Zihao Chen[a] *and Kristen A. Fichthorn*[a,b,*]

[a]Department of Chemical Engineering, Pennsylvania State University, University Park, PA 16802 (USA)

[b]Department of Physics, Pennsylvania State University, University Park, PA 16802 (USA)

*Kristen A. Fichthorn (fichthorn@psu.edu)

Abstract

We used dispersion-corrected density-functional theory to perform an *in silico* search over a series of primary alkylamines, including linear, branched, and cyclic molecules, to identify capping molecules for shape-selective Cu nanocrystal synthesis. We identify several attributes associated with successful capping agents. Generally, molecules with good geometric matching to the Cu surfaces possessed the strongest molecule-surface chemical bonds. However, non-bonding van der Waals interactions and molecular packing constraints can play a more significant role in determining the overall binding energy, the surface coverage, and the likely efficacy of the capping molecule. Though nearly all the molecules exhibited stronger binding to Cu(100) than to Cu(111), all predicted Wulff shapes are primarily {111}-faceted, based on *ab initio* thermodynamics calculations. From predicted capping-molecule densities on Cu(100) and Cu(111) for various solution environments, we identified several candidate molecules to produce {100}- or {111}-faceted nanocrystals with kinetic shapes, based on synthesis conditions used to grow Cu nanowires with ethylenediamine capping agent. Our study reveals the complexity of capping-molecule binding and important considerations that go into the selection of a successful capping agent.

1. Introduction

Metal nanocrystals feature in a number of cutting-edge applications including catalysis[1,2], electronic devices[3,4], energy storage[5,6], and fuel cells[7,8]. For these and many more applications, it has been emphasized that performance is largely determined by the nanocrystal morphology.[9–15] Although many investigators have demonstrated the capability to produce nanocrystals with a variety of shapes,[16,17] it remains a challenge to achieve high and selective yields to particular nanocrystal morphologies.

In solution-phase syntheses, capping agents are important for achieving shape control and there are many studies linking particular crystal shapes to particular capping agents.[17] For example, Yu et al. studied the influence of amino acids with different functional groups on the morphologies of Cu nanocrystals and found that different shapes could be synthesized, depending on the molecule.[18] Polyvinylpyrrolidone (PVP) has been linked to the formation of {100}-faceted Ag nanocrystals, while citric acid is linked to {111}-faceted Ag crystals.[19] Chloride and linear alkylamines have been linked to the formation of Cu nanowires,[20–24] while iodide and hexadecylamine (HDA) are associated with Cu microplates.[25] Studies such as these (and many more[17]) indicate the possibility to design optimal capping agents to target particular nanostructures, which is the goal of the present study.

We investigate the influence of molecular structure on the interfacial properties of primary alkylamines on Cu(100) and Cu(111) surfaces using first-principles, dispersion-corrected density-functional theory (DFT). We limit our focus to the {100} and {111} surfaces because these are the primary facets in structures of interest, including penta-twinned Cu nanowires,[20–24] microplates,[25] and single-crystal structures, such as cubes.[22] In prior work, we found that HDA and ethylenediamine (EDA), bind to Cu(100) and Cu(111) with their nitrogen atoms directly above

a Cu atom.[26,27] Moreover, the Cu-N bond was localized to an amine group, while the charge distribution in the rest of the molecule is virtually unchanged due to bonding. As we will discuss below, this is also the case for the alkylamines studied here, so we can vary the adsorption properties of such molecules by tuning their size and the placement of amine groups to match the symmetry of the underlying Cu surface.

In DFT calculations, we consider the binding of capping molecules to single-crystal surfaces in a zero-temperature, vacuum environment. Thus, we neglect many complexities of solution-phase syntheses, in which solvent, solution-phase additives, and various choices of processing conditions can also affect the outcome of a synthesis. There is a growing body of evidence that DFT calculations can indicate successful capping agents in experiments based on capping-molecule binding, alone.[20,25–39] Thus, we pursue the appealing prospect that DFT calculations can indicate trends in solution-phase syntheses.

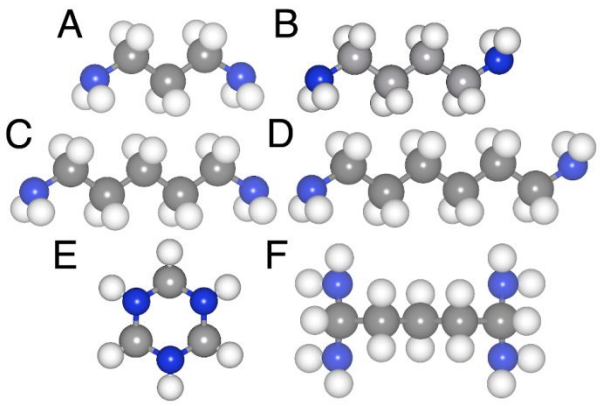

Figure 1. Alkylamine molecules investigated. (**A**) Trimethylenediamine (TrMDA), (**B**) Tetramethylenediamine (TeMDA), (**C**) Pentamethylenediamine (PMDA), (**D**) Hexamethylenediamine (HMDA), (**E**) Pentane-1,1,5,5-Tetramine (PTA), and (**F**) 1,3,5-Triazinane (TZ). Nitrogen is blue, carbon is gray, and hydrogen is white.

We study the series of linear, branched, and cyclic alkylamine candidates depicted in **Figure 1**. We vary the chain length of linear alkylamine diamines to control their symmetry, as well as the alignment of their amine groups with Cu surface atoms. We also study branched and cyclic alkylamines designed to match the structure of the Cu surfaces. While our studies reveal there are structural features of alkylamines that confer surface-selective chemical bonding, we identify several other features of alkylamine binding that are likely important in creating shape-selective nanocrystals.

2. Methods

To identify the influence of the capping molecules in **Figure 1** on shape-selective Cu nanocrystal growth, we investigated their adsorption at various coverages on Cu(100) and Cu(111) using DFT with dispersion corrections. The Vienna *Ab initio* Simulation Package (VASP) was employed for all DFT calculations using the projector-augmented wave pseudopotential method[42–46] and the generalized gradient approximation exchange-correlation functional by Purdue, Burke, and Ernzerhof.[47] More details of the calculations are provided in the ESI, in **Table S1** and pages S2-S3.

We considered adsorption in a coverage window ranging from 0.06 to 0.25 monolayer (ML) on both Cu surfaces, where coverage in ML is defined as the ratio of the number of alkylamine molecules to the number of Cu atoms in the top layer of the slab. To probe the optimized binding configuration of alkylamines on the Cu surfaces, different initial configurations were tested, after which the optimal configuration was identified with the lowest energy. Based on both experimental/theoretical studies for short-chain alkylamines[26,27,41], we probed initial conditions in which the alkylamines were oriented with their long axes parallel to the surface. Different

orientation angles of the long axis with respect to the surfaces [γ – see the Electronic Supporting Information (ESI), p. S3] were probed with $\gamma = 0°$ and $45°$ on Cu(100) and $\gamma = 0°$ and $30°$ on Cu(111). Additionally, different adsorption sites for N, including atop, bridge, and hollow were tested on both Cu(100) and Cu(111). The unit cells used for each coverage are given in **Table S1**.

Several energetic measures were used to characterize alkylamine adsorption on the Cu surfaces. The total binding energy E_{bind} is given by

$$E_{\mathrm{bind}} = (N_{\mathrm{Ads}}E_{\mathrm{Ads}} + E_{\mathrm{Cu}} - E_{\mathrm{Cu-Nads}})/N_{\mathrm{Ads}}, \quad (1)$$

where E_{Ads} and N_{Ads} are the optimized gas-phase energy and number of the adsorbed molecules, while E_{Cu} and $E_{\mathrm{Cu-Nads}}$ are the energy of the optimal bare Cu slab and optimal adsorption system containing N_{Ads} molecules, respectively. The total binding energy can be further broken down into the sum of three types of interactions, such that

$$E_{\mathrm{bind}} = E_{\mathrm{Ads-Ads}} + E_{\mathrm{Cu-Ads}} + \Delta E_{\mathrm{Cu}}. \quad (2)$$

Formulae for each of the terms in Equation (2) are given in the ESI. Since we account for dispersion interactions in our calculations, all the energetic quantities in Equation (2) can be partitioned into two different components: the long-range van der Waals (vdW) interaction and the short-range interaction. The short-range interaction between the adsorbed molecules and the Cu surface characterizes the strength of the chemical bond between them. We also evaluated several geometric characteristics of the alkylamine adlayers and these are discussed in the ESI (See **Figure S1**).

3. Results and Discussion

3.1 Linear Aliphatic Diamines

We investigated linear aliphatic diamines with three to six C atoms in the chain and amine groups on the first and last carbon. By varying the chain length and molecular symmetry, we can manipulate the alignment between bound N atoms and Cu surface atoms to achieve geometric matching. The odd-numbered alkylamines studied are trimethylenediamine (TrMDA) and pentamethylenediamine (PMDA) (cf., **Figure 1A** and **1C**). These molecules can bind in configurations for which both amine groups reside in close proximity to Cu surface atoms when the carbon backbone is oriented either parallel or perpendicular to the surface. Thus, we tested both initial configurations (see **Figures S2A** and **S2B**). The break-down in binding energies for the pattern with the highest binding energy at each coverage is summarized in **Figure 2** and the energy values can be found in **Table S2**. In **Table S3**, we present key geometric features of the TrMDA and PMDA adlayers with the highest binding energies on Cu(100) and Cu(111). Top-down views of these adlayers are shown in **Figure S3.**

Figure 2 indicates the largest contribution to the overall binding energy E_{bind} of TrMDA and PMDA molecules is $E_{\mathrm{Cu-Ads}}$. The highest binding energy for TrMDA on Cu(100) occurs at 0.08 ML coverage (see **Figure 2A**), where $E_{\mathrm{Cu-Ads}}$ is higher than $E_{\mathrm{bind}}$and $E_{\mathrm{Ads-Ads}}$ is overall negative. TrMDA has good matching with Cu(100) at 0.08 ML, so that both amine groups reside on top of Cu surface atoms. As a consequence, TrMDA forms two Cu-N bonds (see the inset to Figure **2A**) with $d^{1}_{\mathrm{N-Cu}} = d^{2}_{\mathrm{N-Cu}} =$ 2.14 Å, where $d^{\mathrm{i}}_{\mathrm{N-Cu}}$ is the distance between nitrogen *i* and the closest Cu(100) surface atom. The strength of these two bonds is reflected in the relatively large short-range component of $E_{\mathrm{Cu-Ads}}$.

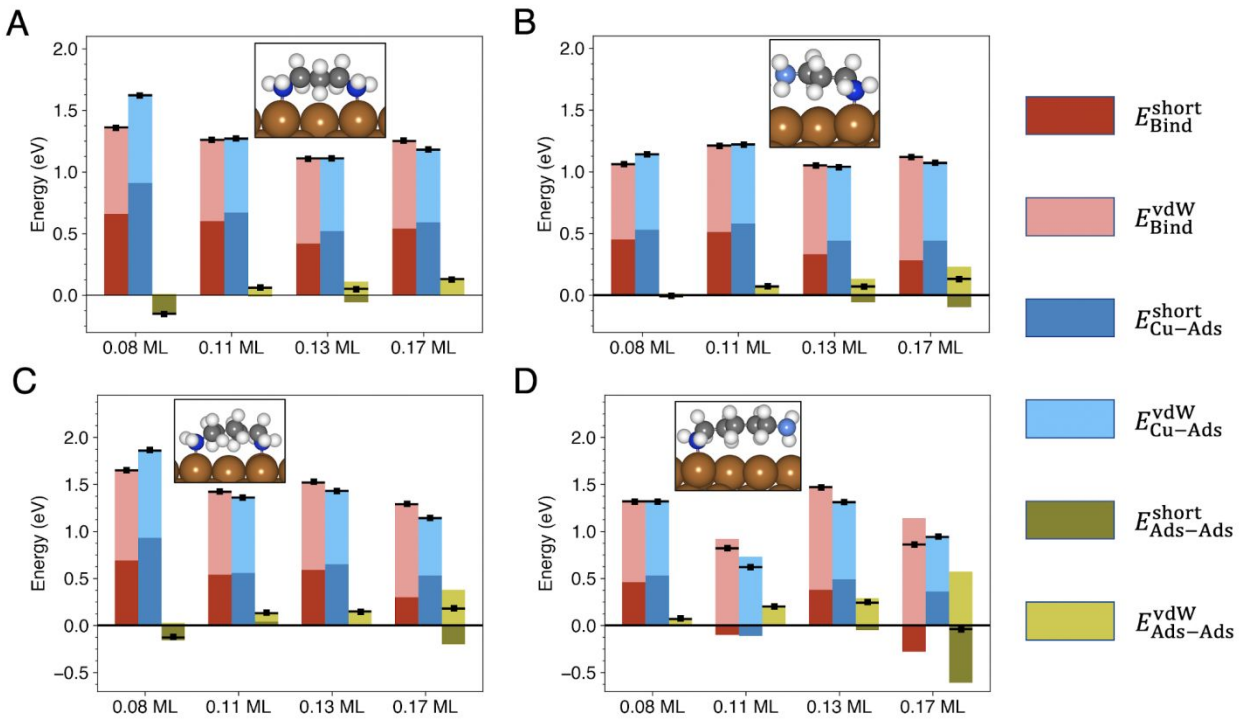

Figure 2. Values of E_{bind} (Equation 2), $E_{\mathrm{Ads-Ads}}$ (Equation S1), and $E_{\mathrm{Cu-Ads}}$ (Equation S2) with a break-down into short-range and vdW components at different coverages for (**A**) TrMDA on Cu(100), (**B**) TrMDA on Cu(111), (**C**) PMDA on Cu(100), and (**D**) PMDA on Cu(111). The total value for each quantity is indicated by the black line with symbol. The insets show sides view of the optimal configurations. Chemisorbed nitrogen is dark blue (with bonds to Cu shown), physisorbed N is light blue, carbon is gray, hydrogen is white, and Cu is brown.

As we see in **Figure 2A**, the short-range component of $E_{\mathrm{Ads-Ads}}$ is negative for TrMDA at 0.08 ML on Cu(100) because the N-N distance in the adsorbed configuration shrinks from 5.09 Å in the gas-phase to 4.83 Å to align both N atoms on top of surface atoms on Cu(100). Thus, a higher TrMDA binding energy is achieved at the energetic cost of a distorted structure. We found one other case with two Cu-N bonds for TrMDA at the same coverage, but with a different orientation angle (see **Figure S2C**) and a lower overall binding energy. Although TrMDA

configurations at other coverages possess a larger value of $E_{\mathrm{Ads-Ads}}$ from stronger inter-molecular vdW interactions, $E_{\mathrm{Cu-Ads}}$ is much weaker. This is because only one Cu-N bond is formed at higher coverages, due to the need to balance geometric matching with the Cu(100) surface and molecular packing constraints.

On Cu(111), the optimal coverage for TrMDA is 0.11 ML and only one Cu-N bond is formed with the Cu surface, as we see in the inset to **Figure 2B**. Cu(111) has weaker short-range and vdW components for $E_{\mathrm{Cu-Ads}}$ than Cu(100) as a result of TrMDA having one bond with the surface instead of two. There is less distortion of the molecule in this configuration than for the optimal configuration on Cu(100), as reflected in the N-N distance of 4.93 Å [*vs.* 4.83 Å on Cu(100)] , resulting in a less negative intra-molecular interaction. At the lowest coverage of 0.08 ML, there is weaker vdW attraction between adsorbed TrMDA molecules, leading to a lower total binding energy. The structures at higher coverages with stronger vdW interaction are not preferred, as the short-range component of $E_{\mathrm{Ads-Ads}}$ is more negative with increasing coverage, indicating more structural distortion as a result of molecular packing constraints.

The binding of PMDA to Cu surfaces shows a similar scenario to TrMDA, in that PDMA also forms two Cu-N bonds in its optimal binding configuration at 0.08 ML on Cu(100) (see the inset to **Figure 2C**), with a similar value for the short-range component of $E_{\mathrm{Cu-Ads}}$. As we saw for TrMDA, the molecular backbone is compressed from 7.64 Å in the gas phase to 7.26 Å when PDMA adsorbs on Cu(100) at this coverage, leading to a negative intra-molecular interaction (reflected in the short-range component of $E_{\mathrm{Ads-Ads}}$). The vdW component of $E_{\mathrm{Cu-Ads}}$ is larger for PMDA than TrMDA because of its larger size. A zigzag pattern at 0.13 ML on Cu(100) has the second highest binding energy among all structures (See **Figure S2D and Table S2**). The

zigzag pattern has a higher intermolecular vdW interaction but only one Cu-N bond per molecule. Similarly, structures at higher coverages have an overall lower binding energy, as they only form one Cu-N bond, even with a much stronger intermolecular vdW interaction. At the highest coverage of 0.17 ML, the short-range component of $E_{\mathrm{Ads-Ads}}$ is negative – likely a consequence of tight molecular packing at this relatively high coverage.

The highest binding energy for PMDA on Cu(111) occurs at a coverage of 0.13 ML. There is one Cu-N bond for this configuration. Despite a relatively strong inter-molecular vdW interaction and less distortion in the molecular structure [N-N distance of 7.39 Å vs. 7.26 Å for Cu(100)], the overall interaction between PMDA and Cu(111) is lower than the optimal case on Cu(100).

Thus, the most strongly bound structures for TrMDA and PMDA on Cu(100) occur when good geometric matching is achieved between the amine groups and the Cu surface atoms, such that these molecules form two N-Cu bonds with the surface. The molecules distort their structure to attain two Cu-N bonds at the expense of the intra-molecular energy. However, the energy gained from surface bonding overcomes the structural energy loss. The matching between these two molecules and Cu(111) is much worse than for Cu(100), as the lengths of their backbones cannot match the distance between any pair of Cu(111) surface atoms, so two bonds do not form upon adsorption.

As candidate molecules with even numbers of C atoms, we studied tetramethylenediamine (TeMDA) (**Figure 1B**) and hexamethylenediamine (HMDA) (**Figure 1D**). Since these molecules lack axial symmetry, we only considered conformations in which the plane of the carbon backbone is parallel to the surface, as perpendicular configurations result in one of the N atoms residing far from the surface. We also tested possible "vertical" configurations for HMDA conformations on

both surfaces (see **Figure S4A** and **S4B**), since linear alkylamines with more than six carbons have been experimentally observed to form self-assembled monolayers with their backbones perpendicular to the surface.[41] However, these 'vertical' conformations are significantly less favored than 'horizontal' conformations. The energy break-down for patterns with the highest binding energy at each coverage is shown in **Figure 3** with detailed values tabulated in **Table S4**. **Table S5** gives a summary of TeMDA and HMDA structures with the highest binding energies and **Figure S5** shows the adlayer structures.

From **Figure 3A**, we see the highest binding energy for TeMDA on Cu(100) occurs at 0.17 ML. TeMDA forms only one bond with Cu(100) at this coverage, with $d^1_{\mathrm{N-Cu}}$= 2.12 Å and $d^2_{\mathrm{N-Cu}}$ = 3.33 Å. Although TeMDA forms two bonds with Cu(100) and has a high value of $E_{\mathrm{Cu-Ads}}$ at 0.08 ML (**Figure S4C**), this occurs at the expense of significant molecular distortion, so this binding configuration is not optimal overall. In its optimal coverage on Cu(111) (0.11 ML), TeMDA also forms just one bond, as we see in **Figure 3B**. TeMDA has a binding preference for Cu(100) and the advantage arises from higher inter-molecular vdW interactions ($E_{\mathrm{Ads-Ads}}$) on Cu(100) at the higher coverage.

The optimal binding of HMDA on Cu(100) occurs at 0.13 ML, with one Cu-N bond, a relatively strong inter-molecular vdW interaction, and significant intra-molecular interaction (see **Figure 3C**). Despite its lack of geometric matching, HMDA has the highest binding energy to Cu(100) of all the linear alkylamines studied because of its strong intermolecular and molecule-surface vdW interactions. Similar to TeMDA, structures at lower coverages possess lower vdW interactions. HMDA forms two Cu-N bonds with Cu(100) at 0.06 ML coverage (**Figure S4D**), but the increased binding energy from the extra bond cannot compensate for intra-molecular distortion

and the weaker vdW interaction at low coverages. The binding energy of HMDA on Cu(111) is in general lower than that on Cu(100). As we see in the inset to **Figure 3D**, HMDA forms only one bond at its optimal coverage of 0.08 ML on Cu(111).

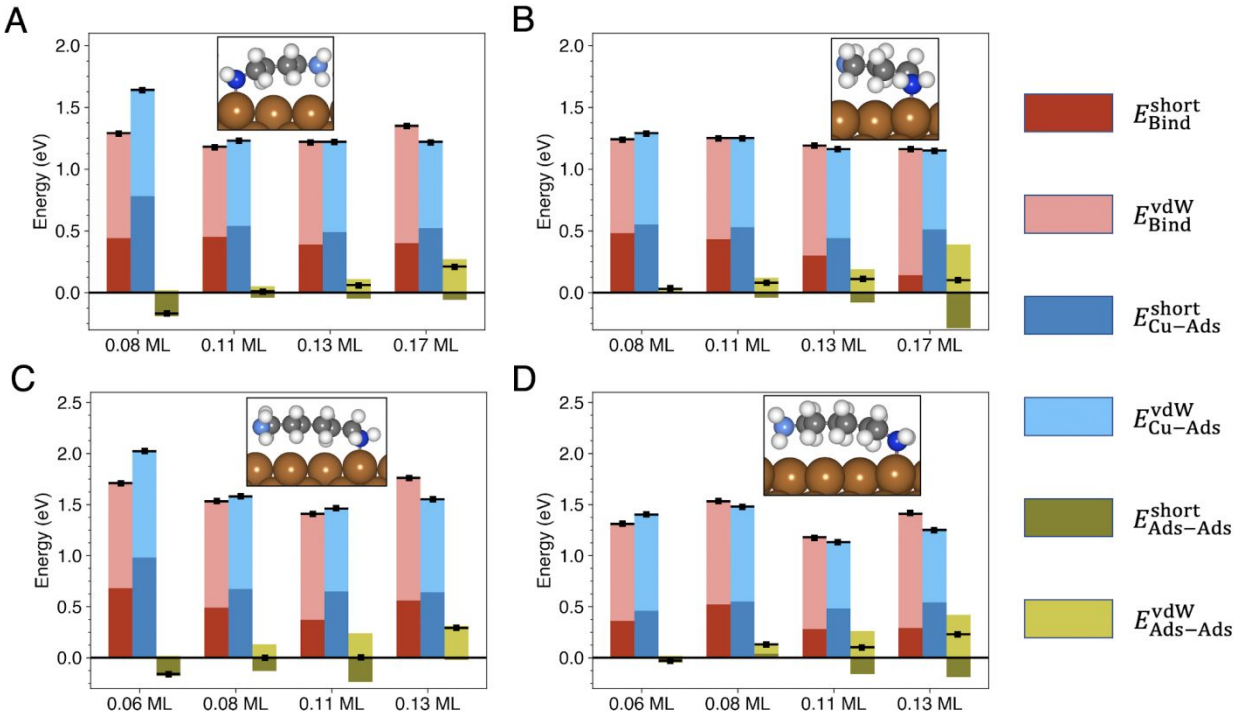

Figure 3. Values of E_{bind} (Equation 2), $E_{\mathrm{Ads-Ads}}$ (Equation S1), and $E_{\mathrm{Cu-Ads}}$ (Equation S2) with a break-down into short-range and vdW components at different coverages for (**A**) TeMDA on Cu(100), (**B**) TeMDA on Cu(111), (**C**) HMDA on Cu(100), and (**D**) HMDA on Cu(111). The total value for each quantity is indicated by the black line with symbol. The insets show sides view of the optimal configurations. Chemisorbed nitrogen is dark blue (with bonds to Cu shown), physisorbed N is light blue, carbon is gray, hydrogen is white, and Cu is brown.

Overall, several features contribute to the binding efficacy of these molecules. Linear aliphatic diamines (TrMDA, PMDA) with an odd number of carbons achieve the best matching of their N atoms with the surface atoms of Cu(100). As a result, these molecules form two chemical bonds

with Cu(100) surface atoms and they possess the strongest molecule-surface interaction ($E_{\mathrm{Cu-Ads}}$) of all the linear molecules studied. The enhanced molecule-surface interaction, even in the case with the best matching, comes at the expense of molecular distortion and the energy cost of this distortion, reflected in the short-range component of $E_{\mathrm{Ads-Ads}}$, is detrimental to the overall binding energy. Despite this detriment, the linear aliphatic diamines with an odd number of carbons bind more strongly to Cu(100) than to Cu(111), largely because of their geometric matching with Cu(100).

The linear aliphatic diamines with an even number of carbons all possess one Cu-N bond at their optimal coverages. For these molecules, geometric matching of both N atoms with the surface was achieved only with considerable molecular distortion. The stronger vdW interactions and less intramolecular distortion associated with having just one Cu-N bond made these binding configurations favorable and endowed HMDA with the highest binding energy of all the linear alkylamines studied.

3.2 Branched and Cyclic Alkylamines

To further explore the impact of geometric matching on facet-selective binding, we considered non-linear molecules with structures designed to match the Cu surface geometries. We chose pentane-1,1,5,5-tetramine (PTA) (see **Figure 1E**) to match Cu(100). PTA has a rectangular structure, in which all four N atoms can reside above Cu(100) surface atoms with minimal structural distortion. We chose triangular 1,3,5-triazinane (TZ) (see **Figure 1F**) to match Cu(111). Detailed values for the breakdown in the binding energies at different coverages of PTA and TZ are given in **Table S6** and **Figure 4** provides a graphical depiction of this information.

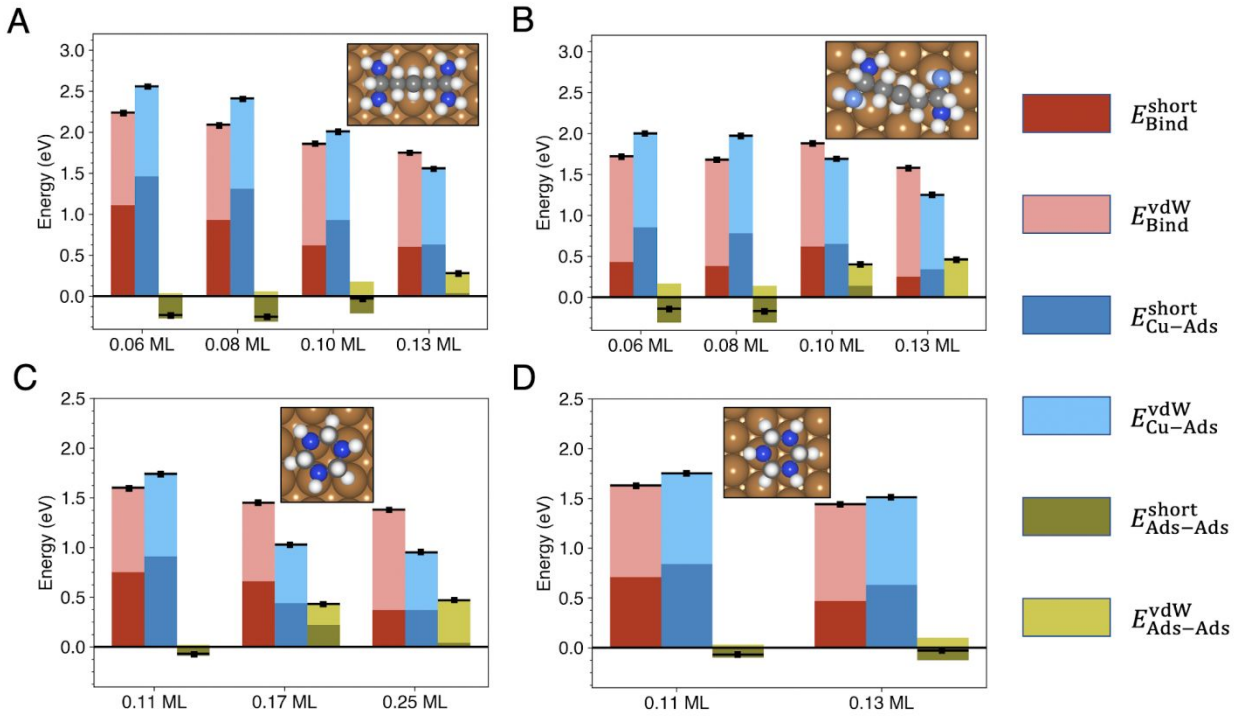

Figure 4. Values of E_{bind} (Equation 2), $E_{\mathrm{Ads-Ads}}$ (Equation S1), and $E_{\mathrm{Cu-Ads}}$ (Equation S2) with a break-down into short-range and vdW components at different coverages for (**A**) PTA on Cu(100), (**B**) PTA on Cu(111), (**C**) TZ on Cu(100), and (**D**) TZ on Cu(111). The total value for each quantity is indicated by the black line with symbol. The insets show top-down views of the optimal configurations. Chemisorbed nitrogen is dark blue, physisorbed N is light blue, carbon is gray, hydrogen is white, and Cu is brown.

With a rectangular arrangement of its amine groups, all four N atoms in PTA can locate on top of Cu(100) surface atoms (see **Figures 4A** and **S6A**) with only slight structural distortion. As a result, PTA exhibits the highest binding energy to Cu(100) of all the candidates investigated, as well as the highest bond strength ($E_{\mathrm{Cu-Ads}}$ in **Figure 4A**) at a coverage of 0.06 ML. Increasing the coverage from the optimal value, molecular packing constraints influence binding and PTA either forms four Cu-N bonds with a significantly twisted structure and a negative intramolecular

interaction (at 0.08 ML coverage) or it has less Cu-N bonds to accommodate the closer distances between molecules (i.e., 0.13 ML coverage with two Cu-N bonds).

The structure of PTA does not match well with Cu(111). With visible distortions in the backbone shown in **Figures 4B** and **S6B**, PTA only forms two Cu-N bonds on Cu(111) and the bond strength, reflected in the short-range component of $E_{\mathrm{Cu-Ads}}$ in **Figure 4A**, is less than half of that on Cu(100) (**Figure 4B**) at the optimal coverage of 0.10 ML. PTA at lower coverages on Cu(111) can form four bonds at the expense of intra-molecular distortion and weaker inter-molecular interaction. However, the bond strength is weaker than on Cu(100).

TZ is the only candidate with a binding preference for Cu(111), as it can have all three N atoms bound without significant distortion (see **Figures 4D** and **S6D**). The binding energy breakdown for TZ is similar on both Cu surfaces (see **Figure 4D**). On Cu(100), one of the Cu atoms bound to an N moves significantly from its original position to form a Cu-N bond, such that there is a significant energy loss in the Cu slab after binding (i.e., ΔE_{Cu} in Equation 2 is non-negligible). It is notable that we could reach a higher coverage of TZ on Cu(100) than on Cu(111) (0.25 ML vs. 0.13 ML) with a zigzag pattern (see **Figure S7**). The binding is not as strong, with only one Cu-N bond formed, as shown in **Figure 4C**, but the inter-molecular vdW interaction contributes greatly in this densely packed layer. We also investigated an alternative boat conformation of TZ, which is less favored than the chair conformation investigated above. This structure has worse matching with Cu(111), such that the bond strength and vdW interaction are both lower as the molecule is more tilted away from the surface with two Cu-N bonds (see **Figure S8**).

The matching of PTA and TZ to the Cu surfaces is also reflected in the projected density of states (PDOS) of their binding on Cu(100) and Cu(111), respectively (see **Figure S9**). The PDOS

is almost identical for each of the four N atoms in PTA on Cu(100). For TZ on Cu(111), the frontier orbitals containing lone-pair electrons from the three nitrogen atoms are identical in both energy levels and the density of states before and after binding, revealing the three-fold symmetric structure in gas phase and excellent matching with Cu(111) after binding.

3.3 Comparison of Alkylamines from ab initio Thermodynamics

To understand the thermodynamic effect of the alkylamines in **Figure 1** on nanocrystal shape, we used *ab initio* thermodynamics calculations to determine capping-molecule-induced Cu surface energies. The surface energy of Cu with adsorbed capping molecules $\gamma_{\mathrm{Cu-Ads}}$ is given by

$$\gamma_{\mathrm{Cu-Ads}} = \frac{E_{\mathrm{Cu-Nads}} - N_{\mathrm{Cu}} E_{\mathrm{Cu}}^{\mathrm{bulk}} - N_{\mathrm{Ads}} \mu_{\mathrm{Ads}}}{A_{\mathrm{surf}}} - \gamma_{\mathrm{Cu}}^{\mathrm{fixed}}. \quad (3)$$

Here, N_{Cu} and $E_{\mathrm{Cu}}^{\mathrm{bulk}}$ represent the number of Cu atoms in the slab and the energy of one bulk Cu atom. μ_{Ads} is the chemical potential of the molecule and A_{surf} is the surface area of one side of the slab. With the one-sided adsorption model used here, we subtracted the surface energy of a fixed Cu surface $\gamma_{\mathrm{Cu}}^{\mathrm{fixed}}$ from the total surface energy of the slab. $\gamma_{\mathrm{Cu}}^{\mathrm{fixed}}$ is given by

$$\gamma_{\mathrm{Cu}}^{\mathrm{fixed}} = \frac{E_{\mathrm{slab,\,fixed}} - N_{\mathrm{Cu}} E_{\mathrm{Cu}}^{\mathrm{bulk}}}{2A_{\mathrm{surf}}}, \quad (4)$$

where $E_{\mathrm{slab,\,fixed}}$ is the total energy of a Cu slab with all of the atoms fixed at the bulk positions. We note that Equations 3 and 4 account for the solution environment through the value of the chemical potential – the influence of the solvent on $E_{\mathrm{Cu-Nads}}$ is not taken into account. We expect the surface free energies to assume lower values when solvent is taken into account explicitly.[37] However, since the capping molecules in our study bind to the Cu surfaces more strongly than water (the presumed solvent) and since these molecules are largely hydrophobic, we expect the

capping molecules to reside the closest and interact the most strongly with the surfaces. It seems unlikely that the secondary effects of solvent would cause the relative energies of the {100} and {111} surfaces to be substantially different than we find here.

Using Equations (3) and (4), we calculated the surface energies of Cu(100) and Cu(111) with all the alkylamines in **Figure 1** as a function of μ_{Ads} with all the capping-molecule coverages represented in **Figures 2–4**. **Figure S10** shows the results and indicates alkylamine adsorption lowers the surface energies and the surface-energy difference between Cu(100) and Cu(111). However, none of the alkylamines could lead to a lower surface energy for Cu(100) than Cu(111). Thus, none of these capping molecules provides a thermodynamic driving force for the formation of {100}-faceted Cu nanocrystals. Similar results were found for EDA and HDA adsorption on Cu surfaces.[26,27,34]

Even though the alkylamine capping molecules cannot impart a thermodynamic preference for {100}-faceted Cu nanostructures, it is still possible for them to mediate {100}-faceted kinetic shapes and there is evidence for this in the literature – e.g., see the summary in reference[48]. Our search for possible kinetic structures includes two considerations, both based on synthesis conditions for Cu nanowires mediated by EDA.[49] First, we consider the need for alkylamine capping molecules to protect Cu surfaces from oxidation. This means we search for alkylamines that achieve a high surface coverage on at least one facet. Second, we consider that differences in alkylamine coverage on the {100} and {111} facets could promote different oxidation rates on the facets, as is believed to occur when EDA is used as a capping molecule.[27,49] Thus, we also searched for alkylamines with a surface-coverage difference between the two facets.

To identify the conditions leading to a high surface coverage and/or a surface-coverage difference between the two facets, we consider each unique pair of minimum-energy surface configurations on Cu(100) and Cu(111) for various values of μ_{Ads} in **Figure S10**. The vertical double arrows in **Figure S10** delineate all the unique surface pairs. For example, TrMDA in **Figure S10A** has five unique Cu(100)/Cu(111) surface pairs, as indicated by the five vertical double arrows. As a measure of the capability of an alkylamine to provide surface protection for a given pair of surfaces, we introduce the occupancy ratio (*OR*). The *OR* is defined for each of the surface pairs in **Figure S10** as

$$OR_{111} = \frac{N_{\mathrm{C},111} + N_{\mathrm{N},111}}{N_{\mathrm{Cu},111}}, \quad (5)$$

and

$$OR_{100} = \frac{N_{\mathrm{C},100} + N_{\mathrm{N},100}}{N_{\mathrm{Cu},100} \cdot A_{100/111}}. \quad (6)$$

Here, $N_{\mathrm{C},111}$ and $N_{\mathrm{C},100}$ are the numbers of C atoms, $N_{\mathrm{N},111}$ and $N_{\mathrm{N},100}$ are the number of N atoms, and $N_{\mathrm{Cu},111}$ and $N_{\mathrm{Cu},100}$ the numbers of Cu atoms in the top layer of the {111} and {100} unit cells, respectively. $A_{100/111}(= 2/\sqrt{3})$ is the surface area ratio of {100} to {111} with the same number of Cu atoms. The *OR* provides a measure of the overall density of alkylamine molecules on each of the thermodynamically preferred surfaces for a fixed chemical potential and we expect the best surface protection for the largest *OR* values.

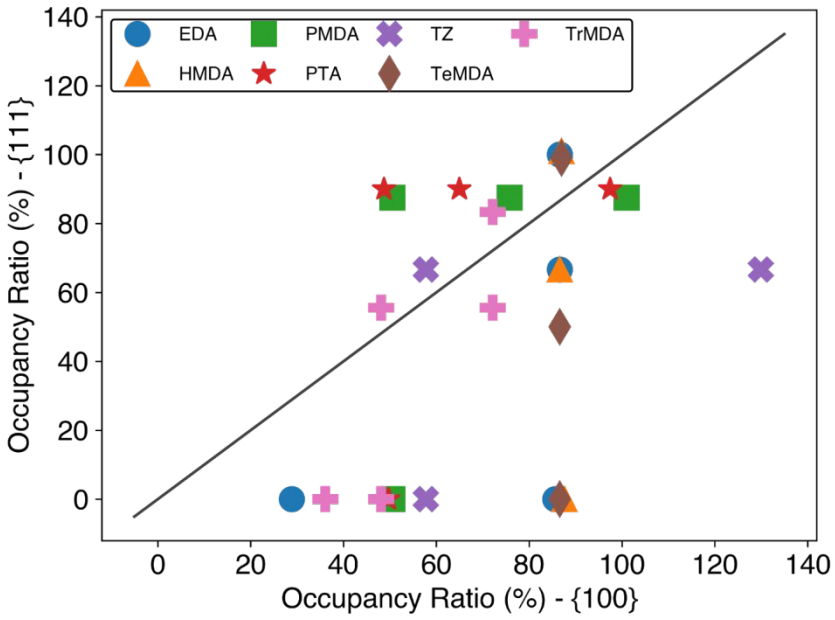

Figure 5. The occupancy ratio of the capping-molecule candidates on Cu(111), given by Equation 5, versus the occupancy ratio on Cu(100), given by Equation 6. Each point reflects a unique pair of {100}/{111} surface configurations, shown by the vertical double arrows in **Figure S10**. The results for EDA are taken from ref. 27.

Figure 5 shows a plot of OR_{111} vs. OR_{100}, where each point reflects a pair of surface configurations indicated by the vertical double arrows in **Figure S10**. The diagonal line in **Figure 5** is where $OR_{111} = OR_{100}$. If $OR_{111} > OR_{100}$, then Cu(111) has a higher capping-molecule density than Cu(100) and if $OR_{100} > OR_{111}$, then Cu(100) has a higher density.

One feature in **Figure 5** (and in **Figure S10**) is that every species exhibits a chemical potential region for which $OR_{111} = 0$ and OR_{100} is finite, meaning Cu(100) is protected by capping agent to some degree and there is no capping agent adsorbed on Cu(111). This is a direct consequence of the lower surface energy of Cu(111) and the larger binding energy per area on Cu(100), as can be seen from Equation (3). Since OR_{100} is relatively low for these points, it seems neither facet

has adequate protection from oxidation or deposition of Cu ions. However, in an environment that does not cause Cu oxidation, such as with co-adsorption of a halide,[20] this could facilitate the growth of {100}-faceted nanostructures by promoting a higher deposition rate to Cu(111) than Cu(100). In particular, high values of OR_{100} occur in the HDA and Cl^- mediated synthesis of Cu nanowires, where Cu(100) is selectively protected by both these species while Cu(111) only has Cl^- adsorbed.[20,50] We note that many syntheses for Cu nanoshapes rely on a $CuCl_2$ salt, so chlorine co-adsorption is a significant consideration.[20–22]

EDA is a reference point in **Figure 5** because there is experimental data indicating EDA promotes penta-twinned nanowire formation.[49] In the experimental synthesis with EDA capping agent, $Cu(NO_3)_2$ salt is used and Cu(100) is selectively oxidized, which promotes nanowire formation. At the highest chemical potential/OR for EDA, $OR_{111} > OR_{100}$ and DFT calculations indicate the barrier for water to pass through the EDA layer on Cu(100) is substantially lower than the barrier on Cu(111).[27] The relatively low value of OR_{100} could lead to oxidation of Cu(100), consistent with experiment.[49] The highest OR_{111} values and corresponding OR_{100} values for TeMDA and HMDA in **Figure 5** are nearly identical to those for EDA. Thus, we could expect similar behavior of these molecules to EDA as capping agents in syntheses with $Cu(NO_3)_2$ salt – they could protect Cu(111), while allowing for oxidation of Cu(100), leading to {100}-faceted nanostructures, such as penta-twinned nanowires. Interestingly, all three of these molecules have an even number of carbons and none of them forms two bonds with the Cu surfaces in their optimal coverages.

Another interesting feature from **Figure 5** is that the highest OR_{100} of PMDA and PTA indicate these species achieve a higher coverage on Cu(100) than on Cu(111). The values of OR_{111} and OR_{100} are essentially reversed compared to the highest values for EDA, TeMDA, and HMDA.

Again, based on results from EDA-mediated Cu nanowire synthesis with $Cu(NO_3)_2$ salt we could anticipate selective oxidation of Cu(111) and {111}-faceted nanostructures. Finally, although TZ achieves nearly perfect geometric matching and exhibits the strongest binding to Cu(111) at its optimal coverage, this molecule achieves the highest OR_{100} of all the molecules studied. Following the lead from experimental studies of EDA-mediated nanowire synthesis, we expect the dense TZ surface coverage implied by this high value of OR_{100} would afford effective surface protection for Cu(100), while allowing for the oxidation of Cu(111). In this case, packing constraints on Cu(111) and the strong inter-molecular vdW interactions that could be achieved on Cu(100) make TZ likely to be an effective capping molecule for achieving {111}-faceted nanostructures.

4. Conclusion

In summary, we used dispersion-corrected DFT to investigate a series of primary alkylamine diamines, including linear, branched, and cyclic molecules, as potential capping molecules for Cu surfaces. In this series, chemical bonding is localized to amine nitrogen atoms and single Cu surface atoms (i.e., the atop sites) of Cu(100) and Cu(111). This enabled us to test the hypothesis that geometric matching between the alkylamine and the Cu atoms in a particular crystalline facet could lead to stronger binding and effectiveness of the molecule as a capping molecule for that facet. Generally, molecules that have good geometric matching with the surfaces, so the amine nitrogen atoms could reside on top of Cu surface atoms, possessed the strongest chemical bonds with the surfaces. However, non-bonding vdW interactions and molecular packing constraints can play a significant role in determining the overall binding energy, the surface coverage, and the likely efficacy of the capping molecule. For example, although HMDA could only form one Cu-

N bond on Cu(100), this linear molecule possessed a higher binding energy to Cu(100) than linear molecules with two Cu-N bonds because of its strong vdW interaction with the surface.

Although all of the molecules studied except for one exhibited stronger binding to Cu(100) than to Cu(111), the facet-selective binding was not strong enough to induce lower surface energies for Cu(100) than for Cu(111). Thus, none of these molecules could induce thermodynamic, {100}-faceted Wulff shapes. Taking inspiration from literature examples, in which differences in the capping-molecule densities on different facets could be correlated to kinetic nanocrystal shapes, we devised the *OR* to assess the capping molecule density on Cu(100) and Cu(111). We used relative *OR* values for pairs of surfaces in the same chemical environment, characterized by the chemical potential, to gauge the relative capping-molecule coverages of the surfaces and the likelihood that a capping molecule could induce kinetic nanocrystal shapes with preferred facets.

Based on *OR* values, we identified several candidate molecules to produce {100}-faceted nanocrystals with kinetic shapes. The literature tells us that EDA mediates Cu nanowire growth because it allows for oxidation of Cu(100), but not Cu(111) as a consequence of its lower density on Cu(100).[27,49] If the density of adsorbed molecules alone is a good indicator of capping ability, then two other molecules, TeMDA and HMDA, may facilitate the growth of primarily {100}-faceted Cu nanowires as EDA does. Following EDA synthesis protocols, we predict PMDA and PTA could be advantageous for producing {111}-faceted nanostructures. These two molecules also exhibit high binding energies as a result of their geometric matching to Cu(100) and would afford better protection from oxidation of Cu(100). TZ, a molecule possessing close geometric matching and favorable binding to Cu(111), achieved highest surface density on Cu(100) of all the molecules studied and shows promise as a capping agent for {111}-faceted Cu nanoshapes following synthesis protocols similar to those used with EDA capping agent.

Thus, we identified several factors, related to and in addition to facet-selective binding, which may portend the capability of a capping molecule to actuate nanocrystal shape formation in solution-phase syntheses. Our discussion of and predictions of capping-molecule function were based on synthesis conditions similar to those used to grow Cu nanowires in aqueous solution using $Cu(NO_3)_2$ salt and EDA capping agent, where selective oxidation of one facet or another could lead to shape preference.[49] We note that such syntheses are relevant for achieving selectivity and stability toward C_{2+} products in the catalytic CO_2 reduction reaction.[51] Our findings could be relevant (albeit with different conclusions regarding shape) for syntheses run under conditions that do not lead to Cu surface oxidation. Though the veracity of our predictions has yet to be confirmed experimentally, our studies reveal the complexity of capping molecule binding and some of the many considerations that go into the design of a successful capping agent.

Acknowledgements

This work was supported by the Department of Energy, Office of Basic Energy Sciences, Materials Science Division, DE-FG02-07ER46414. Z.C. acknowledges training provided by the Computational Materials Education and Training (CoMET) NSF Research Traineeship (DGE-1449785).

References

(1) Christopher, P.; Linic, S. Engineering Selectivity in Heterogeneous Catalysis: Ag Nanowires as Selective Ethylene Epoxidation Catalysts. *J. Am. Chem. Soc.* **2008**, *130* (34), 11264–11265.

(2) Roberts, F. S.; Kuhl, K. P.; Nilsson, A. High Selectivity for Ethylene from Carbon Dioxide Reduction over Copper Nanocube Electrocatalysts. *Angew. Chemie Int. Ed.* **2015**, *54* (17), 5179–5182.

(3) Hu, L.; Kim, H. S.; Lee, J.-Y.; Peumans, P.; Cui, Y. Scalable Coating and Properties of Transparent, Flexible, Silver Nanowire Electrodes. *ACS Nano* **2010**, *4* (5), 2955–2963.

(4) Rathmell, A. R.; Wiley, B. J. The Synthesis and Coating of Long, Thin Copper Nanowires to Make Flexible, Transparent Conducting Films on Plastic Substrates. *Adv. Mater.* **2011**, *23* (41), 4798–4803.

(5) Li, G.; Kobayashi, H.; Dekura, S.; Ikeda, R.; Kubota, Y.; Kato, K.; Takata, M.; Yamamoto, T.; Matsumura, S.; Kitagawa, H. Shape-Dependent Hydrogen-Storage Properties in Pd Nanocrystals: Which Does Hydrogen Prefer, Octahedron (111) or Cube (100)? *J. Am. Chem. Soc.* **2014**, *136* (29), 10222–10225.

(6) Jena, P. Materials for Hydrogen Storage: Past, Present, and Future. *J. Phys. Chem. Lett.* **2011**, *2* (3), 206–211.

(7) Chen, S.; Gasteiger, H. a.; Hayakawa, K.; Tada, T.; Shao-Horn, Y. Platinum-Alloy Cathode Catalyst Degradation in Proton Exchange Membrane Fuel Cells: Nanometer-Scale Compositional and Morphological Changes. *J. Electrochem. Soc.* **2010**, *157* (1), A82–A97.

(8) You, H.; Yang, S.; Ding, B.; Yang, H. Synthesis of Colloidal Metal and Metal Alloy Nanoparticles for Electrochemical Energy Applications. *Chem. Soc. Rev.* **2013**, *42* (7), 2880–2904.

(9) Xiao, B.; Niu, Z.; Wang, Y.-G.; Jia, W.; Shang, J.; Zhang, L.; Wang, D.; Fu, Y.; Zeng, J.; He, W. Copper Nanocrystal Plane Effect on Stereoselectivity of Catalytic Deoxygenation of Aromatic Epoxides. *J. Am. Chem. Soc.* **2015**, *137* (11), 3791–3794.

(10) Ye, S.; Stewart, I. E.; Chen, Z.; Li, B.; Rathmell, A. R.; Wiley, B. J. How Copper Nanowires Grow and How to Control Their Properties. *Acc. Chem. Res.* **2016**, *49* (3), 442–451.

(11) Chen, T.; Chen, S.; Song, P.; Zhang, Y.; Su, H.; Xu, W.; Zeng, J. Single-Molecule Nanocatalysis Reveals Facet-Dependent Catalytic Kinetics and Dynamics of Pallidium Nanoparticles. *ACS Catal.* **2017**, *7* (4), 2967–2972.

(12) Li, Z.; Ji, S.; Liu, Y.; Cao, X.; Tian, S.; Chen, Y.; Niu, Z.; Li, Y. Well-Defined Materials

for Heterogeneous Catalysis: From Nanoparticles to Isolated Single-Atom Sites. *Chem. Rev.* **2020**, *120* (2), 623–682.

(13) De Gregorio, G. L.; Burdyny, T.; Loiudice, A.; Iyengar, P.; Smith, W. A.; Buonsanti, R. Facet-Dependent Selectivity of Cu Catalysts in Electrochemical CO2 Reduction at Commercially Viable Current Densities. *ACS Catal.* **2020**, *10* (9), 4854–4862.

(14) Zhao, M.; Chen, Z.; Shi, Y.; Hood, Z. D.; Lyu, Z.; Xie, M.; Chi, M.; Xia, Y. Kinetically Controlled Synthesis of Rhodium Nanocrystals with Different Shapes and a Comparison Study of Their Thermal and Catalytic Properties. *J. Am. Chem. Soc.* **2021**, *143* (16), 6293–6302.

(15) Shi, Y.; Lyu, Z.; Zhao, M.; Chen, R.; Nguyen, Q. N.; Xia, Y. Noble-Metal Nanocrystals with Controlled Shapes for Catalytic and Electrocatalytic Applications. *Chemical Reviews*. January 2021, pp 649–735.

(16) Xia, Y.; Xia, X.; Peng, H.-C. C. Shape-Controlled Synthesis of Colloidal Metal Nanocrystals: Thermodynamic versus Kinetic Products. *J. Am. Chem. Soc.* **2015**, *137* (25), 7947–7966.

(17) Yang, T. H.; Shi, Y.; Janssen, A.; Xia, Y. Surface Capping Agents and Their Roles in Shape-Controlled Synthesis of Colloidal Metal Nanocrystals. *Angew. Chemie - Int. Ed.* **2020**, *59* (36), 15378–15401.

(18) Yu, J.-C.; Zhao, F.-G.; Shao, W.; Ge, C.-W.; Li, W.-S. Shape-Controllable and Versatile Synthesis of Copper Nanocrystals with Amino Acids as Capping Agents. *Nanoscale* **2015**, *7* (19), 8811–8818.

(19) Zeng, J.; Zheng, Y.; Rycenga, M.; Tao, J.; Li, Z.-Y.; Zhang, Q.; Zhu, Y.; Xia, Y. Controlling the Shapes of Silver Nanocrystals with Different Capping Agents. *J. Am. Chem. Soc.* **2010**, *132*, 8552–8553.

(20) Kim, M. J.; Alvarez, S.; Chen, Z.; Fichthorn, K. A.; Wiley, B. J. Single-Crystal Electrochemistry Reveals Why Metal Nanowires Grow. *J. Am. Chem. Soc.* **2018**, *140* (44), 14740–14746.

(21) Kim, M. J.; Alvarez, S.; Yan, T.; Tadepalli, V.; Fichthorn, K. A.; Wiley, B. J. Modulating the Growth Rate, Aspect Ratio, and Yield of Copper Nanowires with Alkylamines. *Chem. Mater.* **2018**, *30* (8), 2809–2818.

(22) Jin, M.; He, G.; Zhang, H.; Zeng, J.; Xie, Z.; Xia, Y. Shape-Controlled Synthesis of Copper Nanocrystals in an Aqueous Solution with Glucose as a Reducing Agent and Hexadecylamine as a Capping Agent. *Angew. Chemie - Int. Ed.* **2011**, *50* (45), 10560–10564.

(23) Xu, S.; Sun, X.; Ye, H.; You, T.; Song, X.; Sun, S. Selective Synthesis of Copper Nanoplates and Nanowires via a Surfactant-Assisted Hydrothermal Process. *Mater. Chem. Phys.* **2010**, *120*, 1–5.

(24) Wang, X.; Wang, R.; Shi, L.; Sun, J. Kinetically Controlled Synthesis of Cu Nanowires with Tunable Diameters and Their Applications in Transparent Electrodes. *J. Mater. Chem. C* **2018**, *6* (5), 1048–1056.

(25) Kim, M. J.; Cruz, M. A.; Chen, Z.; Xu, H.; Brown, M.; Fichthorn, K. A.; Wiley, B. J. Isotropic Iodide Adsorption Causes Anisotropic Growth of Copper Microplates. *Chem. Mater.* **2021**, *33* (3), 881–891.

(26) Liu, S.-H. H.; Balankura, T.; Fichthorn, K. A. Self-Assembled Monolayer Structures of Hexadecylamine on Cu Surfaces: Density-Functional Theory. *Phys. Chem. Chem. Phys.* **2016**, *18* (48), 32753–32761.

(27) Chen, Z.; Fichthorn, K. A. Adsorption of Ethylenediamine on Cu Surfaces: Attributes of a Successful Capping Molecule Using First-Principles Calculations. *Nanoscale* **2021**, *13*, 13529–13537.

(28) Kilin, D. S.; Prezhdo, O. V; Xia, Y. Shape-Controlled Synthesis of Silver Nanoparticles: Ab Initio Study of Preferential Surface Coordination with Citric Acid. *Chem. Phys. Lett.* **2008**, *458* (1–3), 113–116.

(29) Zhou, Y.; Saidi, W. A.; Fichthorn, K. A. Comparison of the Binding of Polyvinylpyrrolidone and Polyethylene Oxide to Ag Surfaces: Elements of a Successful Structure-Directing Agent. *J. Phys. Chem. C* **2013**, *117* (21), 11444–11448.

(30) Al-Saidi, W. A.; Feng, H.; Fichthorn, K. A. Adsorption of Polyvinylpyrrolidone on Ag Surfaces: Insight into a Structure-Directing Agent. *Nano Lett.* **2012**, *12* (2), 997–1001.

(31) Saidi, W. A.; Feng, H.; Fichthorn, K. A. Binding of Polyvinylpyrrolidone to Ag Surfaces: Insight into a Structure-Directing Agent from Dispersion-Corrected Density Functional Theory. *J. Phys. Chem. C* **2013**, *117* (2), 1163–1171.

(32) Liu, S. H.; Saidi, W. A.; Zhou, Y.; Fichthorn, K. A. Synthesis of {111}-Faceted Au Nanocrystals Mediated by Polyvinylpyrrolidone: Insights from Density-Functional Theory and Molecular Dynamics. *J. Phys. Chem. C* **2015**, *119* (21), 11982–11990.

(33) Ye, J. Y.; Attard, G. A.; Brew, A.; Zhou, Z. Y.; Sun, S. G.; Morgan, D. J.; Willock, D. J. Explicit Detection of the Mechanism of Platinum Nanoparticle Shape Control by Polyvinylpyrrolidone. *J. Phys. Chem. C* **2016**, *120* (14), 7532–7542.

(34) Fichthorn, K. A.; Chen, Z. Surface Science of Shape-Selective Metal Nanocrystal Synthesis from First-Principles: Growth of Cu Nanowires and Nanocubes. *J. Vac. Sci. Technol. A Vacuum, Surfaces Film.* **2020**, *38* (2).

(35) Chen, Z.; Balankura, T.; Fichthorn, K. A.; Rioux, R. M. Revisiting the Polyol Synthesis of Silver Nanostructures: Role of Chloride in Nanocube Formation. *ACS Nano* **2019**, *13* (100), 1849–1860.

(36) Qi, X.; Balankura, T.; Zhou, Y.; Fichthorn, K. A. How Structure-Directing Agents Control

Nanocrystal Shape: Polyvinylpyrrolidone-Mediated Growth of Ag Nanocubes. *Nano Lett.* **2015**, *15* (11), 7711–7717.

(37) Qi, X.; Fichthorn, K. A. Theory of the Thermodynamic Influence of Solution-Phase Additives in Shape-Controlled Nanocrystal Synthesis. *Nanoscale* **2017**, *9* (40), 15635–15642.

(38) Fichthorn, K. A.; Balankura, T.; Qi, X. Multi-Scale Theory and Simulation of Shape-Selective Nanocrystal Growth. *CrystEngComm* **2016**, *18* (29), 5410–5417.

(39) Liu, S. H.; Fichthorn, K. A. Interaction of Alkylamines with Cu Surfaces: A Metal-Organic Many-Body Force Field. *J. Phys. Chem. C* **2017**, *121* (40), 22531–22541.

(40) Liu, S. H.; Fichthorn, K. A. Interaction of Alkylamines with Cu Surfaces: A Metal-Organic Many-Body Force Field. *J. Phys. Chem. C* **2017**, *121* (40), 22531–22541.

(41) Song, P.; Sangeeth, C. S. S.; Thompson, D.; Du, W.; Loh, K. P.; Nijhuis, C. A. Noncovalent Self-Assembled Monolayers on Graphene as a Highly Stable Platform for Molecular Tunnel Junctions. *Adv. Mater.* **2016**, *28* (4), 631–639.

(42) Blöchl, P. E. Projector Augmented-Wave Method. *Phys. Rev. B* **1994**, *50* (24), 17953–17979.

(43) Kresse, G.; Joubert, D. From Ultrasoft Pseudopotentials to the Projector Augmented-Wave Method. *Phys. Rev. B* **1999**, *59* (3), 1758–1775.

(44) Kresse, G.; Hafner, J. Ab Initio Molecular Dynamics for Liquid Metals. *Phys. Rev. B* **1993**, *47* (1), 558–561.

(45) Kresse, G.; Hafner, J. Ab Initio Molecular-Dynamics Simulation of the Liquid-Metalamorphous- Semiconductor Transition in Germanium. *Phys. Rev. B* **1994**, *49* (20), 14251–14269.

(46) Kresse, G.; Furthmüller, J. Efficient Iterative Schemes for Ab Initio Total-Energy Calculations Using a Plane-Wave Basis Set. *Phys. Rev. B* **1996**, *54* (16), 11169–11186.

(47) Perdew, J. P.; Burke, K.; Ernzerhof, M. Generalized Gradient Approximation Made Simple. *Phys. Rev. Lett.* **1996**, *77* (18), 3865–3868.

(48) Fichthorn, K. A.; Chen, Z.; Chen, Z.; Rioux, R. M.; Kim, M. J.; Wiley, B. J. Understanding the Solution-Phase Growth of Cu and Ag Nanowires and Nanocubes from First Principles. *Langmuir* **2021**, *37*, 4419–4431.

(49) Kim, M. J.; Flowers, P. F.; Stewart, I. E.; Ye, S.; Baek, S.; Kim, J. J.; Wiley, B. J. Ethylenediamine Promotes Cu Nanowire Growth by Inhibiting Oxidation of Cu(111). *J. Am. Chem. Soc.* **2017**, *139* (1), 277–284.

(50) Fichthorn, K. A.; Chen, Z. Surface Science of Shape-Selective Metal Nanocrystal

Synthesis from First-Principles: Growth of Cu Nanowires and Nanocubes. *J. Vac. Sci. Technol. A* **2020**, *38* (2), 023210.

(51) Lyu, Z.; Zhu, S.; Xie, M.; Zhang, Y.; Chen, Z.; Chen, R.; Tian, M.; Chi, M.; Shao, M.; Xia, Y. Controlling the Surface Oxidation of Cu Nanowires Improves Their Catalytic Selectivity and Stability toward C2+ Products in CO2 Reduction. *Angew. Chemie - Int. Ed.* **2021**, *60* (4), 1909–1915.